iScience

CellPress
OPEN ACCESS

Article

Small-molecule fulvic acid with strong hydration ability for non-vitreous cellular cryopreservation

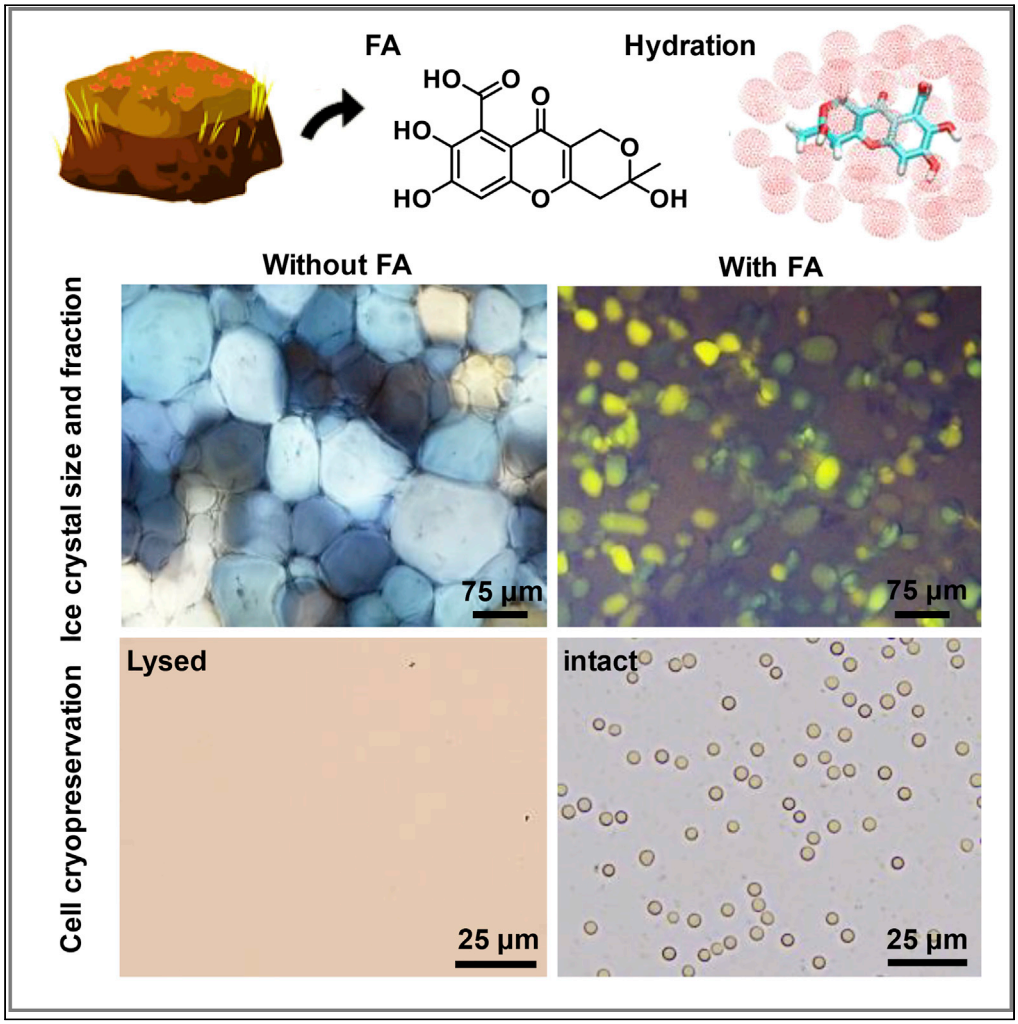

Guoying Bai, Jinhao Hu, Sijia Qin, ..., Shenglin Jin, Dong Gao, Jianjun Wang

baiguoying@iccas.ac.cn (G.B.)
gaodong@iccas.ac.cn (D.G.)

Highlights

FA shows strong hydration ability

FA reduces ice growth/recrystallization and promotes ice melting

FA can be absorbed by RBCs and mainly locates on membranes

FA enables non-vitreous cellular cryopreservation

Bai et al., iScience 25, 104423
June 17, 2022
https://doi.org/10.1016/j.isci.2022.104423

iScience

CellPress
OPEN ACCESS

Article

Small-molecule fulvic acid with strong hydration ability for non-vitreous cellular cryopreservation

Guoying Bai,[1,3,4,*] Jinhao Hu,[1] Sijia Qin,[1] Zipeng Qi,[1] Hening Zhuang,[1] Fude Sun,[2] Youhua Lu,[3] Shenglin Jin,[3] Dong Gao,[2,*] and Jianjun Wang[3]

SUMMARY

The exploitation of biocompatible ice-control materials especially the small molecules for non-vitreous cryopreservation remains challenging. Here, we report a small molecule of fulvic acid (FA) with strong hydration ability, which enables non-vitreous cellular cryopreservation by reducing ice growth during freezing and reducing ice recrystallization/promoting ice melting during thawing. Without adding any other cryoprotectants, FA can enhance the recovery of sheep red blood cells (RBCs) by three times as compared with a commercial cryoprotectant (hydroxyethyl starch) under a stringent test condition. Investigation of water mobility reveals that the ice-control properties of FA can be ascribed to its strong bondage to water molecules. Furthermore, we found that FA can be absorbed by RBCs and mainly locates on membranes, suggesting the possible contribution of FA to cell protection through stabilizing membranes. This work bespeaks a bright future for small-molecule cryoprotectants in non-vitreous cryopreservation application.

INTRODUCTION

Successful cryopreservation of biological materials, which is fundamental for medicine, biology, and agriculture, requires the precise control of ice formation (Biggs et al., 2017; Chang and Zhao, 2021; Pegg, 2007; Zhan et al., 2021). For instance, antifreeze proteins (AFPs) can efficiently protect many overwintering organisms from freezing damage by inhibiting ice growth/recrystallization (Bar Dolev et al., 2016). Compared with the cryopreservation method of vitrification, which needs large amounts of toxic permeable cryoprotectants such as glycerol or dimethyl sulfoxide, as well as fast cooling rates to promote water forming amorphous glass (ice-free) state (Fahy and Wowk, 2021; Zhan et al., 2022), AFP-inspired ice-control strategy is superior in terms of biocompatibility and mass cryopreservation (Deller et al., 2014; Fowler and Toner, 2006). However, despite the excellent ice growth/recrystallization inhibition activity of AFPs, their practical applications in cryopreservation are limited by the high cost and low flexibility of production (Deller et al., 2014). Furthermore, other unique properties of AFPs such as thermal hysteresis (TH) activity and ice-shaping effect also impede their application in cryopreservation, because the uncontrolled sudden burst of spicular ice crystals can damage the cells during freeze-thawing (Carpenter and Hansen, 1992; Chao et al., 1996; O'Neil et al., 1998; Wang et al., 1994). Therefore, a low-cost, biocompatible, ice growth/recrystallization-inhibiting cryopreservation agent without TH/ice-shaping effect is in urgent request (Gibson, 2010).

Over the past decades, more and more materials that can reduce ice growth/recrystallization have been discovered/designed (Ampaw et al., 2019; Bai et al., 2017; Baruch and Mastai, 2007; Budke and Koop, 2006; Corcilius et al., 2013; Deller et al., 2014; Drori et al., 2016; Eniade et al., 2001; Geng et al., 2017; Gibson et al., 2009; Graham et al., 2017, 2018; Inada and Lu, 2003; Li et al., 2019; Mastai et al., 2002; Mitchell et al., 2017; Zhu et al., 2019). One effective strategy is mimicking the adsorption inhibition mechanism of AFP through designing AFP-similar repeated ice-binding/amphiphilic structures. Besides, some works demonstrated the importance of hydration, and proposed the linear correlation between the ice recrystallization activity and the hydration ability of small molecular carbohydrates (Czechura et al., 2008; Klinmalai et al., 2017; Tam et al., 2008), implying an alternative, simple strategy of improving hydration for designing ice growth/recrystallization inhibition materials. Although many ice-control materials were reported and some of them indeed displayed attractive ice growth/recrystallization inhibition abilities, only a part of them showed potential application in cryopreservation area, and very few especially small molecules could

[1]School of Materials Science and Engineering, Hebei University of Technology, Tianjin 300401, China

[2]Key Laboratory of Hebei Province for Molecular Biophysics Institute of Biophysics, Hebei University of Technology, Tianjin 300401, China

[3]Institute of Chemistry, Chinese Academy of Sciences, Beijing 100190, China

[4]Lead contact

*Correspondence: baiguoying@iccas.ac.cn (G.B.), gaodong@iccas.ac.cn (D.G.)

https://doi.org/10.1016/j.isci.2022.104423

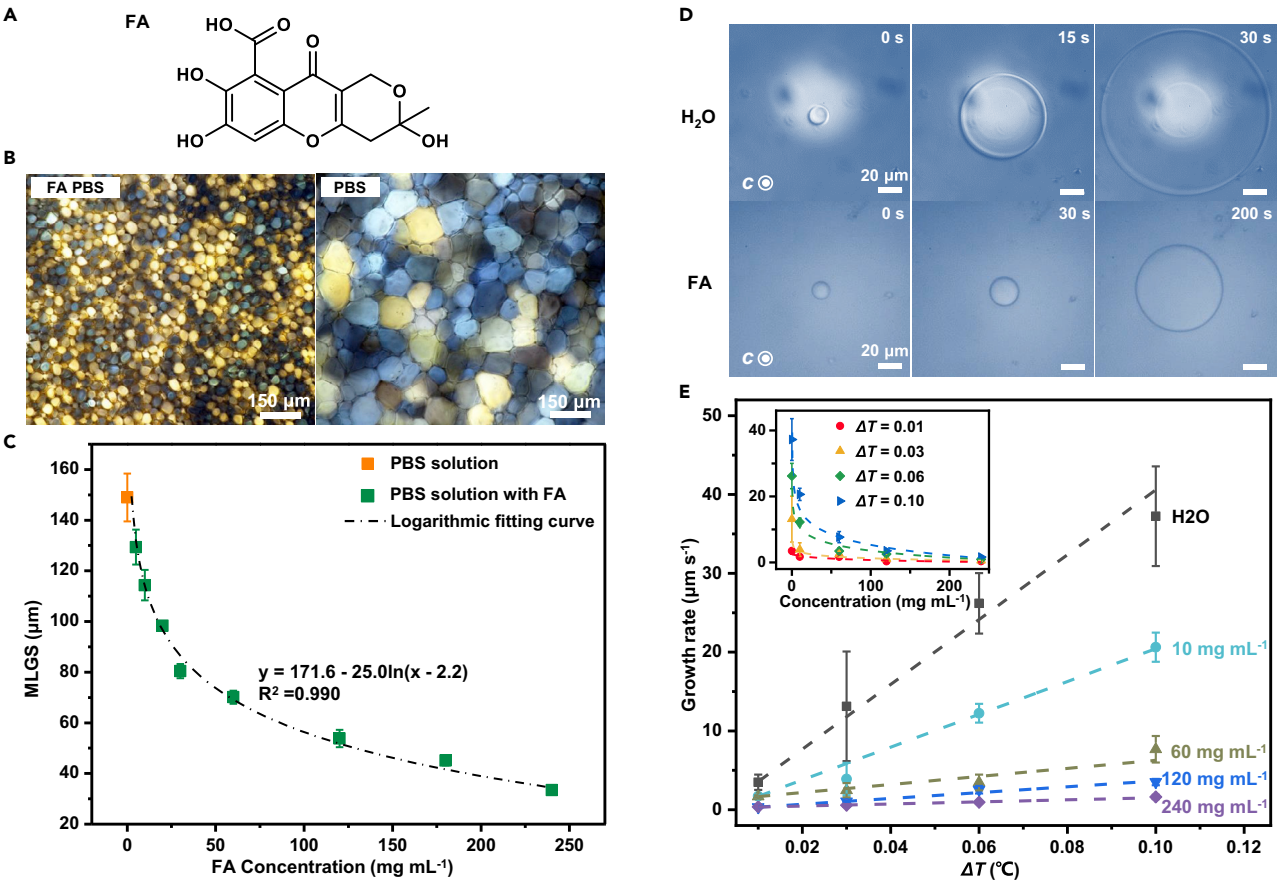

Figure 1. Effect of FA on ice recrystallization/growth/shaping

(A) Acknowledged structure formula of FA.

(B) Polarizing microscope photographs of ice crystals grown in the PBS solution with and without FA (120 mg mL^{-1}) after annealing at − 8°C for 45 min.

(C) Quantitative assessment of the grain size of ice crystals grown in FA PBS solutions of a series of concentrations. To ensure the high fraction of ice during the assay, the annealing temperature was set as − 8°C. Annealing time: 45 min.

(D) Growth processes of single ice crystals in pure water and FA aqueous solution. ΔT was set as 0.01°C to explore whether FA is TH active. The concentration of FA is 120 mg mL^{-1}.

(E) Growth rate variations of ice crystals in FA solutions of various concentrations of ΔT. The dash lines represent the linear fittings of the corresponding data points with the same color. The inset shows the relationships between ice crystal growth rates and FA concentrations under various ΔTs. The dash lines represent the logarithmic fitting of the corresponding data points. All the data are means ± SD.

achieve non-vitreous cell cryopreservation without needing any permeable cryoprotectants such as glycerol and dimethyl sulfoxide.

Here, we discover that a small molecule—fulvic acid (FA) with strong hydration ability—can reduce ice growth/recrystallization, accelerate ice melting, and exhibit no TH/ice-shaping effect. It can achieve non-vitreous cell cryopreservation without need of any other cryoprotectants, displaying a great potential in cryopreservation. FA is a natural health product that comes from humic substances and is rich in carboxyl, hydroxyl, carbonyl, and quinonyl functional groups. Although the structure of FA has been proposed to be a mixture, FA (CAS number: 479-66-3) is consistent with the structure shown in Figure 1A (Winkler and Ghosh, 2018). Traditional medicine and modern research indicate that FA can be absorbed by living organisms, and shows biological activities such as immunemodulation, antioxidant, and antihypertensive effects (Wilson et al., 2011; Winkler and Ghosh, 2018). In addition, FA has been available as a nutraceutical to the public (Pena-Mendez et al., 2005). Owing to the easy accessibility and high biocompatibility of FA, we believe that our finding will greatly promote the utilization of FA or FA-inspired small molecules to non-vitreous cryopreservation.

RESULTS

Effect of FA on ice recrystallization/growth/shaping

As shown in Figures 1B and 1C, we firstly investigated the effect of FA on ice recrystallization via the splat cooling method (Bai et al., 2017; Knight et al., 1988). Typical optical microscopic images (Figure 1B) show that the recrystallized ice crystals in the frozen droplet of FA PBS solution are much smaller than those in the blank control (PBS solution), indicating that FA can reduce ice recrystallization. Further quantitative assessment of the grain size of ice crystals grown in FA solutions with a series of concentrations was performed by measuring the mean largest grain size (MLGS) (see STAR Methods). The results are collected in Figure 1C. It is obvious that FA reduces the grain sizes of recrystallized ice crystals under all the investigated concentrations and higher concentration affords smaller grain size. The fitting curve of the MLGS versus FA concentration indicates the strong logarithmic relationship between the ice recrystallization reduction ability and concentration. The similar non-colligative relationship has also been observed in the case of biological antifreezes (Kumble et al., 2008; Uchida et al., 2007). When the concentration of FA reaches up to 240 mg mL^{-1}, the MLGS can be reduced to *ca.* 20%. Note that such a concentration-dependent ice grain size reduction extent is some better than those achieved by D-galactose and D-melibiose (the most active monosaccharide and disaccharide, respectively (Tam et al., 2008), see Figure S1), and ranked as low/no ice recrystallization inhibition activity compared with the activities of AFPs (Biggs et al., 2019). However, this does not rule out the potential cryopreservation applications of FA, where reducing ice grain size is crucial and high concentrations can be applied (Biggs et al., 2019).

As TH and ice-shaping effect are not desired in cryopreservation, we studied growth behaviors of ice crystals including morphology and growth rate in FA aqueous solution by a nanoliter osmometer (see STAR Methods) to explore whether FA shows TH activity and ice-shaping effect. As shown in Figure 1D, the ice crystal in FA solution presents a flat disk shape, which is exactly the same with that in pure water. This demonstrates that the surface energies of the ice crystal boundary parallel to the *c*-axis are isotropic, *i.e.*, FA cannot adsorb on a certain plane of ice crystal specifically and exhibit no ice-shaping effect (Drori et al., 2016), which is beneficial to the improvement of cryopreservation efficiency. Moreover, under the same ΔT, the ice crystal in FA solution grows much more slowly than that in the pure water, indicating FA's ability in reducing ice growth. Figure 1E summarizes the systematical measurement results about the growth rates of ice crystals in FA solutions of different concentrations under various ΔTs. It is no doubt that the ice crystals in FA solutions of all the investigated concentrations grow much more slowly than those in the pure water under the same ΔT, further verifying FA can reduce ice growth. Note that the ice crystal growth rate increases linearly with the increase of ΔT, suggesting FA exhibits no TH activity. This also avails the enhancement of cryopreservation. Furthermore, with the increase of FA concentration, the ice crystal growth rate decreases in a logarithm tendency (the inset of Figure 1E), which is consistent with the ice recrystallization result (Figure 1C).

Mechanism of FA's slowing ice recrystallization/growth

Adsorption inhibition mechanism is widely accepted as the ice recrystallization/growth inhibition mechanism of AFPs. However, as FA neither present ice-shaping effect nor TH activity, the adsorption inhibition mechanism is unlikely to be applicable here. To verify this, we performed the ice affinity experiment inspired by the AFP purification method (see Figure S2 for the schematic diagram of the apparatus) (Kuiper et al., 2003). Briefly, ice grew on the seeded ice crystal which was immersed into the FA solution under the set temperature and then was collected to measure the concentration of FA in the ice phase. The growth rate of ice was controlled by tuning the set temperature. The results (see Table S1) demonstrate that the FA concentration in ice phase decreases with the increase of set temperature, *i.e.*, the decrease of ice growth rate, and finally becomes too low to be detected. This indicates that FA cannot adsorb preferentially on ice, as the materials such as AFPs, which can adsorb specifically on certain planes of ice crystals, will be concentrated in the ice phase when a solution freezes (Kuiper et al., 2003; Raymond and DeVries, 1977).

To explore the ice recrystallization/growth reduction mechanism of FA, we measured NMR proton spin-spin relaxation time T_2, which strongly depends on water mobility, to investigate the influence of FA on the dynamics of water (McConville and Pope, 2001). Figure 2A shows the peak values of T_2 inversion spectra of water in FA H_2O/PBS solution with a series of concentrations. The detailed T_2 inversion spectra are shown in Figure S3. It is obvious that no matter dissolved in pure water or in PBS solution, FA decreases T_2 of H_2O, suggesting that water mobility is retarded due to FA's bondage to water molecules mainly through hydration (Wu and Chen, 2012; Zhu et al., 2017). Furthermore, with the increase of FA

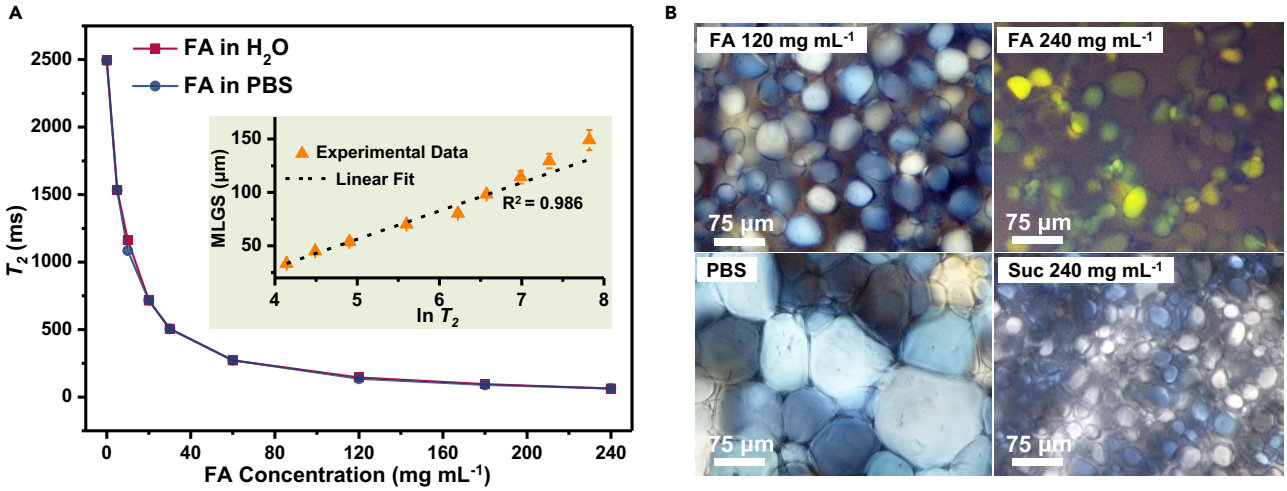

Figure 2. Exploration of ice recrystallization/growth reduction mechanism of FA

(A) The peak values of T_2 inversion spectra of water in FA aqueous/PBS solution of varied concentrations. The inset displays the relationship between MLGS of ice crystals grown in FA PBS solutions and T_2 of water in FA PBS solution. The data are means ± SD.

(B) Polarizing microscope photographs of ice crystals grown in FA PBS solutions of different concentrations, PBS solution, and sucrose PBS solution after annealing at − 6°C for 30 min.

concentration, T_2 decreases logarithmically, which is consistent with the logarithmic variation trend of MLGS versus FA concentration (Figure 1C). The inset of Figure 2A reveals the correlation between MLGS and lnT_2 presents a good linear fitting. For the T_2 values measured under other temperatures, the correlation remains (Figure S4). The strong correlation between MLGS and T_2 indicates that the ice recrystallization/growth reduction mechanism of FA can be ascribed to the bondage of FA to water molecules. This is reasonable by considering that the bondage of FA to water increases the energy associated with transferring a water molecule to the ice lattice, thus slowing the ice recrystallization/growth.

Interestingly, during observing the ice recrystallization process, we found that FA obviously increases the amount of water around the ice crystals. As shown in Figure 2B, dramatically different from the ice crystals in PBS solution, when the concentration of FA is 120 mg mL^{-1}, obvious bulk water surrounding the ice crystals can be observed. With the higher concentration of 240 mg mL^{-1}, only a small percentage of ice crystals are immersed in the bulk water. However, the bulk water is not obvious even when the concentration increases up to 240 mg mL^{-1} for the sucrose (Suc), which is often used to create ice-water balance in the sucrose-sandwich-splat assay (Budke et al., 2009; Smallwood et al., 1999). This indicates the strong hydration ability of FA. By further measuring the T_2 of H_2O in solutions of a series of sugars or typical permeable cryoprotectant dimethyl sulfoxide or macromolecule hydroxyethyl starch (HES) as the controls (Figure S5), we find that the decrease of T_2 for FA is much more than those for the controls, suggesting the superior hydration of FA.

Cryopreservation effect of FA

Based on the effect of FA on slowing ice recrystallization and growth, the effectiveness of FA for cryopreservation of sheep RBCs was investigated. The cytocompatibility of FA was firstly investigated. The results as shown in Figure S6 indicate that FA exhibits no detectable cytotoxicity to sheep RBCs even when the concentration is increased up to 240 mg mL^{-1}. Therefore, FA PBS solutions with a series of concentrations ranging from 10 to 240 mg mL^{-1} were served as the cryoprotectants. Both the mild test condition of fast thawing at 45°C and stringent test condition of slow thawing at 4°C were performed. As shown in Figure 3A, without the addition of any other cryoprotectants, FA of all the investigated concentrations is positive in improving the cell recovery, compared with the PBS blank control sample. Furthermore, the cell recovery rises with the increase of FA concentration and reaches up to around 45% at 4°C thawing condition and 80% at 45°C thawing condition when the applied concentration of FA is 240 mg mL^{-1}. However, the best cell recovery at 4°C thaw for the commercial HES appearing at the concentration of 215 mg mL^{-1} is *ca.* 13%, which is less than a third of that for FA. Because specific element type and content of FA may change slightly with origin regions (Winkler and Ghosh, 2018), we also explored the cryopreservation efficiency

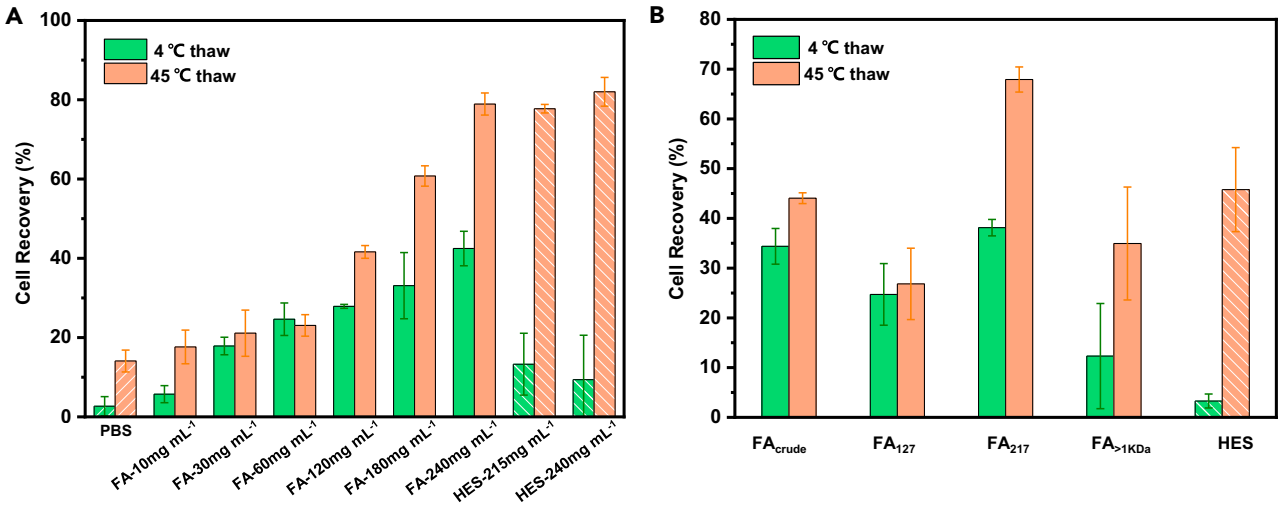

Figure 3. Application of FA for the cryopreservation of sheep RBCs

(A) Recovery of sheep RBCs cryopreserved in FA PBS solutions of different concentrations and thawed at 45°C or 4°C. HES PBS solution is used as the positive control.

(B) Recovery of sheep RBCs cryopreserved with the addition of crude FA and FAs of different molecular weight fractionated from the crude FA. Temperature for thawing: 45°C or 4°C. Sample concentrations: 120 mg mL^{-1}. All the data are means ± SD.

of another FA which contains no nitrogen but a little higher oxygen (Figure S7). As shown in Figure S8, it is also effective in improving the cell recovery, further indicating the cryopreservation availability of FA. The cryopreservation efficiency and ice recrystallization reduction ability of FA were compared with those of representative small-molecule ice recrystallization inhibitors, as shown in Table S2 (Bratosin et al., 2005; Deller et al., 2014; Mitchell et al., 2016; Tam et al., 2008) and Figure S9. Although the ice recrystallization reduction ability of FA is not the top tier, it is a more potent cryoprotectant which can be used alone without adding any permeable cryoprotectants. This suggests that other ice-control properties besides slowing ice growth/recrystallization or some other unknown properties of FA may play an important role in the cell protection, which will be discussed in the following section.

By fractionating the crude FA based on the molecular weight (see STAR Methods), cryopreservation effect can be further improved. As shown in Figure 3B, the three major FA fractions—FA with the molecular weight larger than 1 KDa ($FA_{>1KDa}$) and FA with the number-average molecular weight of 127 (FA_{127}) and 217 (FA_{217}) (see Figure S10 for their chemical structure analysis)—were also used for the RBC cryopreservation without adding any other cryoprotective solvents as the above. With the equally good cytocompatibilities (Figure S11), it is obvious that the second fraction, *i.e.*, FA_{217}, possesses the best cryopreservation effect, which is similar to the effect achieved by using crude FA with double the dosage (240 mg mL^{-1} in Figure 3A) and is far better than the effect of HES under both the fast and slow thaw conditions. Furthermore, because post-thaw culture is usually crucial in the evaluation of new cryoprotectants, the cell recovery (Figure S12) and viability (Figures S13–S15) of RBCs at different post-thaw culturing time were measured. The results suggest that both the cell recovery and cell viability exhibit no decline even after 24 h post-thaw.

Cryopreservation mechanisms of FA

One reason that FA enhances the recovery of cryopreserved RBCs can be ascribed to the effect of FA on slowing ice recrystallization undoubtedly, because ice recrystallization during thawing is a major cause of cell death (Fowler and Toner, 2006). However, we note that having the equivalent effect on ice recrystallization with HES (Figure S16), FA displays better cryopreservation effect than HES especially under the slow thaw (4°C) condition (Figure 3). This suggests that there are other reasons for FA's superior cryopreservation availability. Considering the strong hydration ability of FA and plenty of water around ice crystals during warming (Figure 2B), We measured the melting points of the cryoprotectant solutions via the differential scanning calorimetry (DSC). The small molecule of Suc was also taken as a control. As shown in Figure 4A, it is found that the frozen FA solutions melt much earlier than both HES and Suc solutions under the same conditions. The thawing processes monitored directly through microscope show the same result

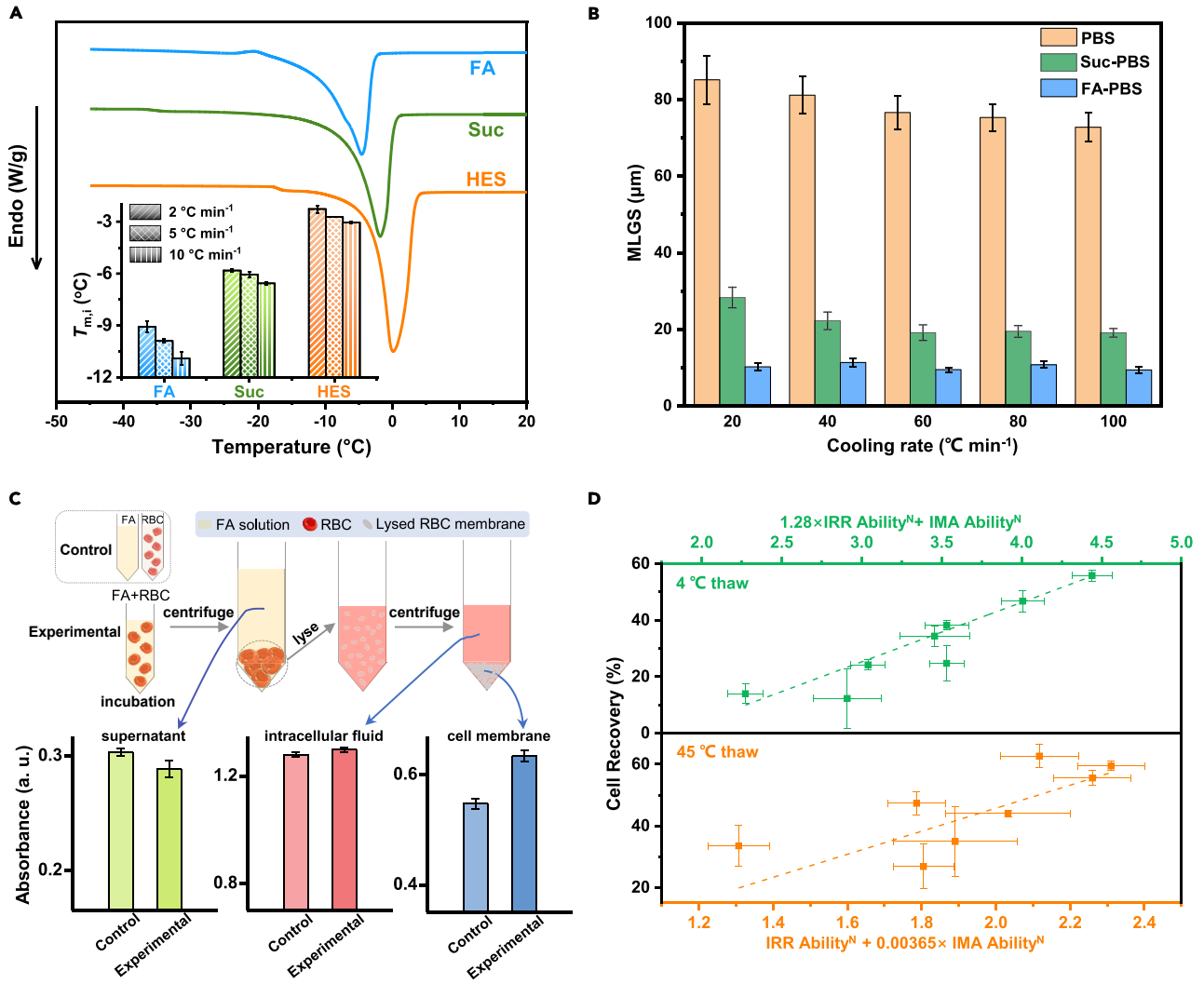

Figure 4. Exploration of cryopreservation mechanisms of FA

(A) Typical DSC of melting of frozen FA (240 mg mL^{-1} ≈ 0.7786 mol L^{-1}), Suc (267 mg mL^{-1} = 0.7786 mol L^{-1}), and HES (240 mg mL^{-1}) PBS droplets under the heating rate of 5°C min^{-1}. The inset shows the initial melting temperature ($T_{m,i}$) of frozen droplets containing various samples under the heating rate of 2, 5, and 10°C min^{-1}.

(B) Grain sizes of ice crystals grown in PBS solutions containing FA or Suc under a series of cooling rates. All sample concentrations are 120 mg mL^{-1}.

(C) Results of FA uptake by RBCs obtained via monitoring the FA absorbance difference between the experimental and control groups. The control group is the same as the experimental group except mixing RBC dispersion with FA solution.

(D) Correlation between the RBC recovery and IRR/IMA ability of various FAs fractions. The detailed data are listed in Table S3. The dash lines represent the linear fittings of the corresponding data points. IRR ability and IMA ability of FA are defined as (1-$MLGS_{FA}/MLGS_{PBS}$)×100%, and 0- $T_{m,i}$, respectively. Note that to compare the relative importance of IRR ability and IMA ability for cryopreservation efficiency, here the IRR or IMA ability are normalized by defining the biggest ability difference between any two FA samples as 1. All the data are means ± SD.

(Figure S17), indicating FA's effectiveness at accelerating ice melting. Note that the ice melting acceleration (IMA) here means the promotion effect of FA on ice melting when the frozen ice is rewarmed. It can also be approximately equivalent to melting point depression, *i.e.*, the ice melts at lower temperatures. Therefore, the IMA ability of FA is also a crucial reason for the cryopreservation enhancement besides ice recrystallization reduction, because IMA reduces the exposure time of cells in ice phase (Manuchehrabadi et al., 2017).

In addition, it is reported that the grain size of extracellular ice crystals during the freezing stage of cryopreservation is also important for the cell recovery (Deller et al., 2014). Therefore, to explore whether FA

contributes to cryopreservation through affecting ice formation during the freezing stage, we measured the grain sizes of ice crystals grown in PBS solutions with and without addition of FA after rapid cooling (typically≥ 20°C min^{-1} to simulate the rapid cooling condition during cryopreservation in this work). The small molecule of Suc was also taken as a control. As shown in Figure 4B, FA greatly reduces the ice crystal grain size from *ca.* 80 μm to *ca.*10 μm under various cooling rates; while, the grain sizes of ice crystals in Suc PBS solutions are ranging from 30 to 20 μm. This indicates that FA can obviously decrease the ice grain size during the freezing stage, which can be ascribed to its ice growth reduction ability (Figure 1E) considering the ice nucleation inertness of small-molecule FA. Therefore, FA's ability of slowing ice growth during freezing stage also contributes to the cryopreservation effect because small ice crystals do not cause extensive damage to cells (Deller et al., 2014).

Furthermore, whether the cryoprotectants permeate into the cells impacts the cryopreservation effect significantly. Therefore, the uptake situation of FA by RBCs was investigated through monitoring the variation of FA concentration. Specifically, as shown in Figure 4C, RBC dispersion mixed with FA solution is set as the experimental group; while, the identical RBC/FA samples without mixing is set as the control group. After incubation for 15 min, both the experimental and control groups were centrifuged, and absorbance of the supernatants were measured and compared to assess whether FA was taken by RBCs. The results (green bars) show that the absorbance of experimental supernatant decreases statistically compared with the control, *i.e.*, FA was taken by the RBCs, resulting in the lower content of FA in the experimental supernatant compared with the control supernatant. By dividing the FA uptake content by the total FA content added (see STAR Methods for the detailed calculation), the uptake ratio of FA by RBCs is about 5% at the dosage condition of 20 mg mL^{-1} FA and 5% RBC. To further explore whether FA attaches on membranes or permeate into RBCs, the obtained precipitates were mixed with pure water to make the RBCs lysed, and then the mixtures were centrifuged at the high speed to separate the intracellular fluid (supernatant) and cell membranes (precipitate). The control group was treated in the same way. Finally, the absorbance values of both the supernatant and precipitate were measured. The results (red bars and blue bars) demonstrate that for supernatant containing intracellular fluid, the experimental group and control group show no significant difference; however, the absorbance of cell membrane precipitate in experimental group is significantly larger than that in control group, suggesting that the absorbed FA by RBCs mainly locates on the cell membranes. This may benefit from the amphipathic character of FA (Mirza et al., 2011; Sanmanee and Areekijseree, 2010). Therefore, the cryopreservation effect of FA may be partially ascribed to its membrane stabilization function besides the ice-control properties (Mirza et al., 2011; Xiao et al., 2018).

Accordingly, the reason of enhanced cryopreservation efficiency of FA fraction (FA_{217}) is further explored, which will contribute to verifying the cryopreservation mechanism of FA. Specifically, different FA fractions' ice growth reduction abilities during freezing (Figure S18), ice recrystallization reduction (IRR) abilities (Figure S19), and IMA abilities (Figure S20) during thawing, and the uptake situations of different FA fractions by RBCs (Figure S21) were investigated. The results show that various FA fractions display comparable ice growth reduction activity during rapid cooling stage, but different IRR and IMA abilities during thawing stage. In addition, all the FA fractions can be taken by RBCs, although the uptake ratios are not identical. By exploring correlation between the above-mentioned properties of FAs and the cell recoveries, we found that IRR and IMA abilities show a good correlation with the cryopreservation efficiency (Figure 4D). This suggests that the influences of different FA fractions on ice crystal grain size and ice melting play the dominant role for their diverse cryopreservation efficiencies—IRR and IMA abilities jointly contribute to improving the cryopreservation efficiency. In addition, note that the contributions of IRR ability and IMA ability on enhancing cell recovery rely on the thaw conditions. Under the slow thaw condition (4°C in refrigerator), where the exposure probability/time of cells in ice phase are relatively larger/longer, the IRR ability and IMA ability contribute comparably to improving the cell recovery. However, under the fast thaw condition of 45°C water bath, where the IMA effect of FA does not exert great breakthrough compared with the fairly fast thaw process, IRR ability plays the dominant role in improving the cryopreservation efficiency. This is of great importance for the design of new cryoprotectants for specific application environments.

Based on the above analyses, the cryopreservation mechanism of FA is proposed. As shown in Figure 5, firstly, during the freezing stage, FA greatly reduces the ice crystal grain size (Figures 1E and 4B), which can alleviate the cell injury because small ice crystals themselves do not cause extensive damage to cells

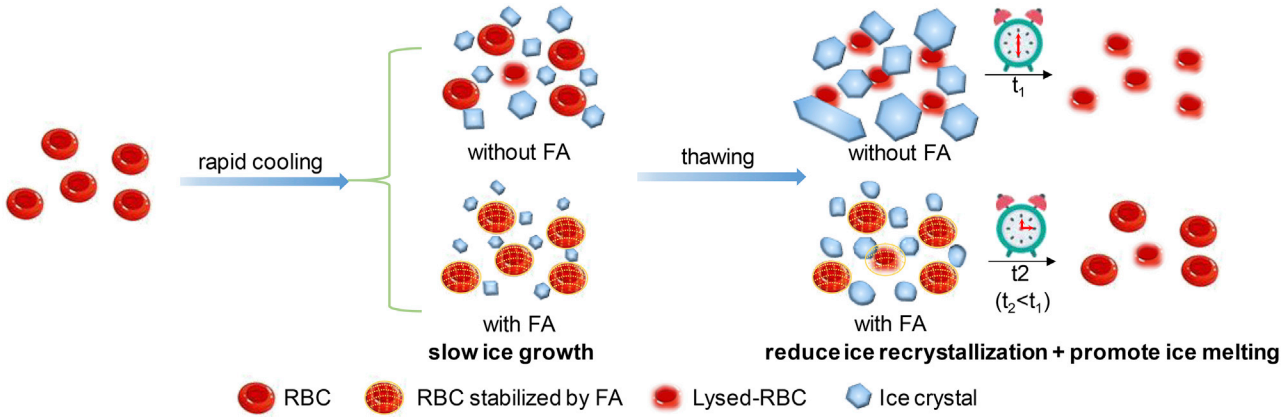

Figure 5. Proposed cryopreservation mechanisms of FA

The proposed mechanisms include 1) decreasing ice grain size through reducing ice growth rate during rapid cooling stage; 2) decreasing ice grain size through reducing ice recrystallization during thawing stage; 3) decreasing exposure time of cells in ice phase and smoothing ice crystals through promoting ice melting during thawing stage; 4) stabilizing cell membranes through membrane absorption of FA.

(Deller et al., 2014). Secondly, during the thawing stage, FA's effect on reducing ice recrystallization (Figure 1C) undoubtedly contributes to enhancing the recovery of cryopreserved RBCs, because ice recrystallization during thawing is a major cause of cell death. Besides, IMA ability of FA (Figure 4A) is another main reason for the improved cell recovery because faster melting reduces the exposure time of cells in ice phase. In addition, the ice crystal images during warming (Figure 2B) suggest that FA significantly reduces the amount of ice crystals, and makes the remained ice crystals smooth without edges and corners, which also help to reduce ice injuries to cells. Finally, the FA uptake experiments reveal that the absorbed FA by RBCs mainly locates on cell membranes (Figure 4C); we propose that the cell protection mechanism of FA may also be related to the membrane absorption of FA, which probably reduces freezing damage to cell membranes.

DISCUSSION

In summary, we discovered a small-molecule cryoprotectant FA with desired ice-control properties including reducing ice growth/recrystallization, accelerating ice melting, and smoothing ice crystal edges, which may all benefit from its strong hydration. It shows excellent biocompatibility, and greatly improves the cell recovery of sheep RBC to more than three times that obtained by using a commercial cryoprotectant—HES without adding any other cryoprotectants such as glycerol or dimethyl sulfoxide. This is a great breakthrough for non-vitreous cryopreservation realized only by a biocompatible small molecule. Further investigation on the correlation between cell recoveries and ice-control abilities of different FA fractions suggests that the properties of reducing ice/recrystallization and accelerating ice melting are indeed related to the cell protection mechanism. Besides, membrane stabilization of FA may also contribute to the high cryopreservation performance. Considering the increasing need for the safer and efficient cryoprotectants, we believe that our finding will greatly promote the utilization of FA or FA-inspired small molecules for cryopreservation. Further investigations with other kinds of cells or tissues will be carried out in the future research.

LIMITATIONS OF THE STUDY

The hydration mechanisms of FA are not very clear in this study. However, we tried to gain more insight into the hydration of FA through all-atom molecular dynamics simulations by respectively solvating one FA and Suc molecule in a water-filled cubic box (see STAR Methods section for details). Analyzed within a 50 ns time duration, the mean square displacement efficiency of the water affected by FA is 26.1 $nm^2\ ns^{-1}$, which is smaller than the value for the case of Suc (27.5 $nm^2\ ns^{-1}$) (Figure S22A). Additionally, the mass density of water surrounding FA and Suc was calculated respectively, and a more remarkable water enrichment within a distance of 4–5 Å around FA is observed (Figure S22B). The simulations thus support the results above revealing the better water immobility restricted by FA. By a further quantization of water number nearby, the water molecules within 5 Å around the mass of center of FA

is 23, which is higher than that of Suc (17) (Figure S22C). It is noteworthy that the water enrichment around FA is heterogeneous in three dimensions and most remarkable along the z axis, corresponding to the evident water distribution on both sides of FA planes (Figure S22D). It provides clues that FA shows higher hydration relying on the specific structure character which may allow a better accessibility of water to FA.

In addition, as FA has been reported to show a variety of biological activities, whether there are other unique abilities of FA that contribute to cellular cryopreservation, *e.g.* the interactions between FA and cells, cannot be excluded. At least, the current experimental results demonstrate that FA can be absorbed on cell membranes, providing the possibility to stabilize membranes. Of course, the cell protection mechanism of FA's absorption on membranes remains to be further verified in the future.

STAR★METHODS

Detailed methods are provided in the online version of this paper and include the following:

- KEY RESOURCES TABLE
- RESOURCE AVAILABILITY
  - Lead contact
  - Materials availability
  - Data and code availability
- METHOD DETAILS
  - Materials
  - Instrumental techniques
  - Ice recrystallization experiments
  - Single ice crystal growth experiments
  - Ice affinity experiments
  - Ice formation observation during rapid cooling stage
  - Fractionation of FA
  - RBC-related experiments
  - Molecular dynamics simulations
  - Statistical analysis

SUPPLEMENTAL INFORMATION

Supplemental information can be found online at https://doi.org/10.1016/j.isci.2022.104423.

ACKNOWLEDGMENTS

The authors acknowledge funding from the National Natural Science Foundation of China (Grant Number 22072036 and 21905072), Natural Science Foundation of Tianjin (Grant Number 20JCQNJC00890), Natural Science Foundation of Hebei Province (Grant Number B2020202034 and B2020202086) and Science and Technology Research Project of Higher Education in Hebei Province (Grant Number BJ2020039).

AUTHOR CONTRIBUTIONS

Conceptualization: G.B., Methodology: G.B., D.G., F.S., J.W., Investigation: G.B., J.H., S.Q., Z.Q., H.Z., Y.L., S.J., D.G., Visualization: G.B., Z.Q., H.Z., Supervision: G.B., Writing—original draft: G.B., Writing—review & editing: G.B., D.G.

DECLARATION OF INTERESTS

The authors declare no competing interests.

Received: March 12, 2022
Revised: April 12, 2022
Accepted: May 11, 2022
Published: June 17, 2022

REFERENCES

Abraham, M.J., Murtola, T., Schulz, R., Páll, S., Smith, J.C., Hess, B., and Lindahl, E. (2015). GROMACS: high performance molecular simulations through multi-level parallelism from laptops to supercomputers. SoftwareX *1–2*, 19–25. https://doi.org/10.1016/j.softx.2015.06.001.

Ampaw, A., Charlton, T.A., Briard, J.G., and Ben, R.N. (2019). Designing the next generation of cryoprotectants - from proteins to small molecules. Pept. Sci. *111*, e24086. https://doi.org/10.1002/pep2.24086.

Bai, G., Song, Z., Geng, H., Gao, D., Liu, K., Wu, S., Rao, W., Guo, L., and Wang, J. (2017). Oxidized Quasi-carbon nitride Quantum dots inhibit ice growth. Adv. Mater. *29*, 1606843. https://doi.org/10.1002/adma.201606843.

Bar Dolev, M., Braslavsky, I., and Davies, P.L. (2016). Ice-binding proteins and their functionR.D. Kornberg, ed. *Vol 85*, 515–542. https://doi.org/10.1146/annurev-biochem-060815-014546.

Baruch, E., and Mastai, Y. (2007). Antifreeze properties of polyglycidol block copolymers. Macromol. Rapid Commun. *28*, 2256–2261. https://doi.org/10.1002/marc.200700501.

Berendsen, H.J.C., Postma, J.P.M., van Gunsteren, W.F., DiNola, A., and Haak, J.R. (1984). Molecular dynamics with coupling to an external bath. J. Chem. Phys. *81*, 3684–3690. https://doi.org/10.1063/1.448118.

Biggs, C.I., Bailey, T.L., Graham, B., Stubbs, C., Fayter, A., and Gibson, M.I. (2017). Polymer mimics of biomacromolecular antifreezes. Nat. Commun. *8*, 1546. https://doi.org/10.1038/s41467-017-01421-7.

Biggs, C.I., Stubbs, C., Graham, B., Fayter, A.E.R., Hasan, M., and Gibson, M.I. (2019). Mimicking the ice recrystallization activity of biological antifreezes. When is a new polymer "active"? Macromol. Biosci. *19*, 1900082. https://doi.org/10.1002/mabi.201900082.

Braslavsky, I., and Drori, R. (2013). LabVIEW-operated novel nanoliter osmometer for ice binding protein investigations. JoVE *72*, e4189. https://doi.org/10.3791/4189.

Bratosin, D., Mitrofan, L., Palii, C., Estaquier, J., and Montreuil, J. (2005). Novel fluorescence assay using calcein-AM for the determination of human erythrocyte viability and aging. Cytometry *66A*, 78–84. https://doi.org/10.1002/cyto.a.20152.

Budke, C., Heggemann, C., Koch, M., Sewald, N., and Koop, T. (2009). Ice recrystallization kinetics in the presence of synthetic antifreeze glycoprotein analogues using the framework of LSW theory. J. Phys. Chem. B *113*, 2865–2873. https://doi.org/10.1021/jp805726e.

Budke, C., and Koop, T. (2006). Ice recrystallization inhibition and molecular recognition of ice faces by poly(vinyl alcohol). ChemPhysChem *7*, 2601–2606. https://doi.org/10.1002/cphc.200600533.

Carpenter, J.F., and Hansen, T.N. (1992). Antifreeze protein modulates cell survival during cryopreservation: mediation through influence on ice crystal growth. Proc. Natl. Acad. Sci. U S A *89*, 8953–8957. https://doi.org/10.1073/pnas.89.19.8953.

Carr, H.Y., and Purcell, E.M. (1954). Effects of diffusion on free precession in nuclear magnetic resonance experiments. Phys. Rev. *94*, 630–638. https://doi.org/10.1103/PhysRev.94.630.

Chang, T., and Zhao, G. (2021). Ice inhibition for cryopreservation: materials, strategies, and challenges. Adv. Sci. *8*, 2002425. https://doi.org/10.1002/advs.202002425.

Chao, H., Davies, P.L., and Carpenter, J.F. (1996). Effects of antifreeze proteins on red blood cell survival during cryopreservation. J. Exp. Biol. *199*, 2071–2076. https://doi.org/10.1242/jeb.199.9.2071.

Corcilius, L., Santhakumar, G., Stone, R.S., Capicciotti, C.J., Joseph, S., Matthews, J.M., Ben, R.N., and Payne, R.J. (2013). Synthesis of peptides and glycopeptides with polyproline II helical topology as potential antifreeze molecules. Bioorg. Med. Chem. *21*, 3569–3581. https://doi.org/10.1016/j.bmc.2013.02.025.

Czechura, P., Tam, R.Y., Dimitrijevic, E., Murphy, A.V., and Ben, R.N. (2008). The importance of hydration for inhibiting ice recrystallization with C-linked antifreeze glycoproteins. J. Am. Chem. Soc. *130*, 2928–2929. https://doi.org/10.1021/ja7103262.

Deller, R.C., Vatish, M., Mitchell, D.A., and Gibson, M.I. (2014). Synthetic polymers enable non-vitreous cellular cryopreservation by reducing ice crystal growth during thawing. Nat. Commun. *5*, 3244. https://doi.org/10.1038/ncomms4244.

Drori, R., Li, C., Hu, C., Raiteri, P., Rohl, A.L., Ward, M.D., and Kahr, B. (2016). A supramolecular ice growth inhibitor. J. Am. Chem. Soc. *138*, 13396–13401. https://doi.org/10.1021/jacs.6b08267.

Eniade, A., Murphy, A.V., Landreau, G., and Ben, R.N. (2001). A general synthesis of structurally diverse building blocks for preparing analogues of C-linked antifreeze glycoproteins. Bioconjugate Chem. *12*, 817–823. https://doi.org/10.1021/bc0155059.

Fahy, G.M., and Wowk, B. (2021). Principles of ice-free cryopreservation by vitrification. Methods Mol. Biol. *2180*, 27–97. https://doi.org/10.1007/978-1-0716-0783-1_2.

Fowler, A., and Toner, M. (2006). Cryo-injury and biopreservation. Ann. N. Y. Acad. Sci. *1066*, 119–135. https://doi.org/10.1196/annals.1363.010.

Geng, H., Liu, X., Shi, G., Bai, G., Ma, J., Chen, J., Wu, Z., Song, Y., Fang, H., and Wang, J. (2017). Graphene oxide restricts growth and recrystallization of ice crystals. Angew. Chem. Int. Ed. *56*, 997–1001. https://doi.org/10.1002/anie.201609230.

Gibson, M.I. (2010). Slowing the growth of ice with synthetic macromolecules: beyond antifreeze(glyco) proteins. Polym. Chem. *1*, 1141–1152. https://doi.org/10.1039/C0PY00089B.

Gibson, M.I., Barker, C.A., Spain, S.G., Albertin, L., and Cameron, N.R. (2009). Inhibition of ice crystal growth by synthetic glycopolymers: implications for the rational design of antifreeze glycoprotein mimics. Biomacromolecules *10*, 328–333. https://doi.org/10.1021/bm801069x.

Graham, B., Bailey, T.L., Healey, J.R.J., Marcellini, M., Deville, S., and Gibson, M.I. (2017). Polyproline as a minimal antifreeze protein mimic that enhances the cryopreservation of cell monolayers. Angew. Chem. Int. Ed. *56*, 15941–15944. https://doi.org/10.1002/anie.201706703.

Graham, B., Fayter, A.E.R., Houston, J.E., Evans, R.C., and Gibson, M.I. (2018). Facially amphipathic glycopolymers inhibit ice recrystallization. J. Am. Chem. Soc. *140*, 5682–5685. https://doi.org/10.1021/jacs.8b02066.

Inada, T., and Lu, S.-S. (2003). Inhibition of recrystallization of ice grains by adsorption of poly(vinyl alcohol) onto ice surfaces. Cryst. Growth Des. *3*, 747–752. https://doi.org/10.1021/cg0340300.

Klinmalai, P., Shibata, M., and Hagiwara, T. (2017). Recrystallization of ice crystals in trehalose solution at isothermal condition. Food Biophys. *12*, 404–411. https://doi.org/10.1007/s11483-017-9496-1.

Knight, C.A., Hallett, J., and DeVries, A.L. (1988). Solute effects on ice recrystallization: an assessment technique. Cryobiology *25*, 55–60. https://doi.org/10.1016/0011-2240(88)90020-X.

Kuiper, M.J., Lankin, C., Gauthier, S.Y., Walker, V.K., and Davies, P.L. (2003). Purification of antifreeze proteins by adsorption to ice. Biochem. Biophys. Res. Commun. *300*, 645–648. https://doi.org/10.1016/S0006-291X(02)02900-5.

Kumble, K.D., Demmer, J., Fish, S., Hall, C., Corrales, S., DeAth, A., Elton, C., Prestidge, R., Luxmanan, S., Marshall, C.J., and Wharton, D.A. (2008). Characterization of a family of ice-active proteins from the Ryegrass, Lolium perenne. Cryobiology *57*, 263–268. https://doi.org/10.1016/j.cryobiol.2008.09.005.

Li, T., Zhao, Y., Zhong, Q., and Wu, T. (2019). Inhibiting ice recrystallization by nanocelluloses. Biomacromolecules *20*, 1667–1674. https://doi.org/10.1021/acs.biomac.9b00027.

Malde, A.K., Zuo, L., Breeze, M., Stroet, M., Poger, D., Nair, P.C., Oostenbrink, C., and Mark, A.E. (2011). An automated force field topology builder (ATB) and repository: version 1.0. J. Chem. Theor. Comput. *7*, 4026–4037. https://doi.org/10.1021/ct200196m.

Manuchehrabadi, N., Gao, Z., Zhang, J., Ring, H.L., Shao, Q., Liu, F., McDermott, M., Fok, A., Rabin, Y., Brockbank, K.G.M., et al. (2017). Improved tissue cryopreservation using inductive heating of magnetic nanoparticles. Sci. Transl. Med. *9*, eaah4586. https://doi.org/10.1126/scitranslmed.aah4586.

Mastai, Y., Rudloff, J., Cölfen, H., and Antonietti, M. (2002). Control over the structure of ice and water by block copolymer additives. ChemPhysChem *3*, 119–123. https://doi.org/10.1002/1439-7641(20020118)3:1<119::AID-CPHC119>3.0.CO;2-R.

McConville, P., and Pope, J.M. (2001). 1H NMR T_2 relaxation in contact lens hydrogels as a probe of water mobility. Polymer *42*, 3559–3568. https://doi.org/10.1016/S0032-3861(00)00714-X.

Meiboom, S., and Gill, D. (1958). Modified spin-echo method for measuring nuclear relaxation times. Rev. Sci. Instrum. *29*, 688–691. https://doi.org/10.1063/1.1716296.

Mirza, M.A., Ahmad, N., Agarwal, S.P., Mahmood, D., Khalid Anwer, M., and Iqbal, Z. (2011). Comparative evaluation of humic substances in oral drug delivery. Results Pharma Sci. *1*, 16–26. https://doi.org/10.1016/j.rinphs.2011.06.001.

Mitchell, D.E., Cameron, N.R., and Gibson, M.I. (2015). Rational, yet simple, design and synthesis of an antifreeze-protein inspired polymer for cellular cryopreservation. Chem. Commun. *51*, 12977–12980. https://doi.org/10.1039/C5CC04647E.

Mitchell, D.E., Clarkson, G., Fox, D.J., Vipond, R.A., Scott, P., and Gibson, M.I. (2017). Antifreeze protein mimetic metallohelices with potent ice recrystallization inhibition activity. J. Am. Chem. Soc. *139*, 9835–9838. https://doi.org/10.1021/jacs.7b05822.

Mitchell, D.E., Lovett, J.R., Armes, S.P., and Gibson, M.I. (2016). Combining biomimetic block copolymer worms with an ice-inhibiting polymer for the solvent-free cryopreservation of red blood cells. Angew. Chem. Int. Ed. *55*, 2801–2804. https://doi.org/10.1002/anie.201511454.

O'Neil, L., Paynter, S.J., Fuller, B.J., Shaw, R.W., and DeVries, A.L. (1998). Vitrification of mature mouse oocytes in a 6 M Me2SO solution supplemented with antifreeze glycoproteins: the effect of temperature. Cryobiology *37*, 59–66. https://doi.org/10.1006/cryo.1998.2098.

Parrinello, M., and Rahman, A. (1981). Polymorphic transitions in single crystals: a new molecular dynamics method. J. Appl. Phys. *52*, 7182–7190. https://doi.org/10.1063/1.328693.

Pegg, D.E. (2007). Principles of cryopreservation. Methods Mol. Biol. *368*, 39–57. https://doi.org/10.1007/978-1-59745-362-2_3.

Peña-Méndez, E.M., Havel, J., and Patocka, J. (2005). Humic substances-compounds of still unknown structure: applications in agriculture, industry, environment, and biomedicine. J. Appl. Biomed. *3*, 13–24. https://doi.org/10.1590/S0101-31222011000200010.

Raymond, J.A., and DeVries, A.L. (1977). Adsorption inhibition as a mechanism of freezing resistance in polar fishes. Proc. Natl. Acad. Sci. U S A *74*, 2589–2593. https://doi.org/10.1073/pnas.74.6.2589.

Sanmanee, N., and Areekijseree, M. (2010). The effects of fulvic acid on copper bioavailability to porcine oviductal epithelial cells. Biol. Trace Elem. Res. *135*, 162–173. https://doi.org/10.1007/s12011-009-8508-5.

Smallwood, M., Worrall, D., Byass, L., Elias, L., Ashford, D., Doucet, C.J., Holt, C., Telford, J., Lillford, P., and Bowles, D.J. (1999). Isolation and characterization of a novel antifreeze protein from carrot (Daucus carota). Biochem. J. *340*, 385–391. https://doi.org/10.1042/0264-6021:3400385.

Stroet, M., Caron, B., Visscher, K.M., Geerke, D.P., Malde, A.K., and Mark, A.E. (2018). Automated topology builder version 3.0: prediction of solvation free enthalpies in water and hexane. J. Chem. Theor. Comput. *14*, 5834–5845. https://doi.org/10.1021/acs.jctc.8b00768.

Tam, R.Y., Ferreira, S.S., Czechura, P., Chaytor, J.L., and Ben, R.N. (2008). Hydration index—a better parameter for explaining small molecule hydration in inhibition of ice recrystallization. J. Am. Chem. Soc. *130*, 17494–17501. https://doi.org/10.1021/ja806284x.

Uchida, T., Nagayama, M., Shibayama, T., and Gohara, K. (2007). Morphological investigations of disaccharide molecules for growth inhibition of ice crystals. J. Cryst. Growth *299*, 125–135. https://doi.org/10.1016/j.jcrysgro.2006.10.261.

Wang, T., Zhu, Q., Yang, X., Layne, J.R., and Devries, A.L. (1994). Antifreeze glycoproteins from antarctic notothenioid fishes fail to protect the rat cardiac explant during hypothermic and freezing preservation. Cryobiology *31*, 185–192. https://doi.org/10.1006/cryo.1994.1022.

Wilson, E., Rajamanickam, G.V., Dubey, G.P., Klose, P., Musial, F., Saha, F.J., Rampp, T., Michalsen, A., and Dobos, G.J. (2011). Review on shilajit used in traditional Indian medicine. J. Ethnopharmacol. *136*, 1–9. https://doi.org/10.1016/j.jep.2011.04.033.

Winkler, J., and Ghosh, S. (2018). Therapeutic potential of fulvic acid in chronic inflammatory diseases and diabetes. J. Diabetes Res. *2018*, 1. https://doi.org/10.1155/2018/5391014.

Wu, J., and Chen, S. (2012). Investigation of the hydration of nonfouling material poly(ethylene glycol) by low-field nuclear magnetic resonance. Langmuir *28*, 2137–2144. https://doi.org/10.1021/la203827h.

Xiao, Y., Wu, Z., and Wang, M. (2018). Effects of fulvic acids on goat sperm. Zygote *26*, 220–223. https://doi.org/10.1017/s0967199418000126.

Zhan, L., Li, M.-g., Hays, T., and Bischof, J. (2021). Cryopreservation method for Drosophila melanogaster embryos. Nat. Commun. *12*, 2412. https://doi.org/10.1038/s41467-021-22694-z.

Zhan, L., Rao, J.S., Sethia, N., Slama, M.Q., Han, Z., Tobolt, D., Etheridge, M., Peterson, Q.P., Dutcher, C.S., Bischof, J.C., and Finger, E.B. (2022). Pancreatic islet cryopreservation by vitrification achieves high viability, function, recovery and clinical scalability for transplantation. Nat. Med. *28*, 798–808. https://doi.org/10.1038/s41591-022-01718-1.

Zhu, W., Guo, J., Agola, J.O., Croissant, J.G., Wang, Z., Shang, J., Coker, E., Motevalli, B., Zimpel, A., Wuttke, S., and Brinker, C.J. (2019). Metal-organic framework nanoparticle-assisted cryopreservation of red blood cells. J. Am. Chem. Soc. *141*, 7789–7796. https://doi.org/10.1021/jacs.9b00992.

Zhu, Z., Xiang, J., Wang, J., and Qiu, D. (2017). Effect of polyvinyl alcohol on ice formation in the presence of a liquid/solid interface. Langmuir *33*, 191–196. https://doi.org/10.1021/acs.langmuir.6b03374.

Zimmerman, J.R., and Brittin, W.E. (1957). Nuclear magnetic resonance studies in multiple phase systems: lifetime of a water molecule in an adsorbing phase on silica gel. J. Phys. Chem. *61*, 1328–1333. https://doi.org/10.1021/j150556a015.

STAR★METHODS

KEY RESOURCES TABLE

REAGENT or RESOURCE	SOURCE	IDENTIFIER
Chemicals, peptides, and recombinant proteins		
Fulvic acid (≥95%)	Shanghai yiyan Biotechnology	CAS: 479-66-3
Phosphate buffered saline (PBS)	Sigma-Aldrich	CAT: 2810305
Hydroxyethyl starch (HES)	Aladdin	CAS: 9005-27-0
D-galactose (>98%)	Alfa Aesar	CAS: 59-23-4
D-(+)-Melibiose Monohydrate (>99%)	TCI	CAS: 66009-10-7
Sucrose (99.9%)	J&K Scientific	CAS:57-50-1
Acetoxymethyl ester of calcein	Solarbio Science & Technology	CAS:1461-15-0
Biological samples		
Sterile sheep RBCs	Solarbio Science & Technology	QS008

RESOURCE AVAILABILITY

Lead contact

Further information and requests for resources and reagents should be directed to and will be fulfilled by the Lead contact, Guoying Bai (baiguoying@iccas.ac.cn).

Materials availability

This study did not generate new unique materials.

Data and code availability

- All data reported in this paper will be shared by the lead contact upon request.
- This paper does not report original code.
- Any additional information required to reanalyze the data reported in this paper is available from the lead contact upon request.

METHOD DETAILS

Materials

Biochemical reagent fulvic acid with the purity of ≥95% was used as obtained from Shanghai yiyan Biotechnology Co., Ltd. (Shanghai, China). For contrast, Another FA purchased from Macklin Biochemical Co., Ltd. (Shanghai, China) was also used. Phosphate buffered saline (PBS) solution was prepared by dissolving one PBS tablet (Sigma-Aldrich) in 200 mL of sterile ultrapure water, yielding 0.01 mol L^{-1} phosphate buffer, 0.137 mol L^{-1} NaCl and 0.0027 mol L^{-1} KCl with the pH of 7.4 at 25°C. Hydroxyethyl starch was used as obtained from Aladdin (Shanghai, China). Its mean molecular weight is 130 kD and the degree of substitution, defined as the average number of hydroxyethyl groups per glucose moiety, is 0.4. D-galactose (>98%), D-melibiose (>99%) and Sucrose (99.9%) were purchased from Alfa Aesar (China) Chemical Co., Ltd., TCI Co., Ltd. (Shanghai, China), and J&K Scientific Ltd. (Beijing, China), respectively. Ultrapure water with a resistivity of 18.2 MΩ cm was obtained from a Millipore Milli-Q apparatus and filtered through a 0.22 μm membrane. Acetoxymethyl ester of calcein (calcein-AM) (2 mM in PBS buffer, stored in −20°C) was purchased from Solarbio Science & Technology Co., Ltd. (Beijing, China). Sterile sheep RBCs (defibrinated, packed cell volume of 20%, stored in Alsever's solution) were purchased on demand from Solarbio Science & Technology Co., Ltd. (Beijing, China). All the cell culture-related solutions were prepared in an ultra-clean bench.

Instrumental techniques

Cooling and heating stage used for the ice recrystallization inhibition investigation was a LTS420 Linkam cryostage with the temperature range of −196 to 420°C and the temperature precision of 0.1°C (Linkam Scientific Instruments Ltd, England). Microscope used for observing the ice crystals was a Nikon AZ100 polarized optical microscope fitted with a digital camera (Nikon DS-Ri1, Nikon, Japan). The growth of single ice crystal was realized by an Otago Nanoliter Osmometer (Otago Osmometers Ltd., Dunedin, New Zealand) with a precision of 0.01°C. The growth process and the morphology of single ice crystals were monitored by a high-speed camera (Phantom V7.3, AMETEK Inc., America). The NMR spin−spin relaxation (T_2) measurements were taken on a low field NMR spectrometer (NMI20-Analyst, Suzhou Numag Analytical Instrument corporation, China) operating at a magnetic field strength of 0.5 ± 0.05 T, corresponding to a proton resonance frequency of 20 MHz. Before measurement, calibrations of center frequency O1, 90° pulse length P1 and 180° pulse length P2 were firstly performed using the Free Induced Decay (FID) single pulse sequence. T_2 was measured using the Carr–Purcell–Meiboom–Gill (CPMG) pulse sequence(Carr and Purcell, 1954; Meiboom and Gill, 1958). The echo time (TE) was 1.5 ms. The number of echo (NECH) was 18000, and the waiting time between two repeated samplings (TW) was 27 s. Generally, the relaxation measurements were performed at 32°C. Besides, the measurements during low temperatures were also realized by a home-made temperature regulating device with samples in a Dewar insulated drivepipe. The inverse analysis was performed by the Numag NMR analysis application software Ver4.0. Specifically, the spin-spin T_2 inversion result was obtained based on the Equation 1 (Zimmerman and Brittin, 1957).

$$M(t) = \sum_i A_i \exp\left(-\frac{t}{T_{2i}}\right) \quad \text{Equation 1}$$

A_i and T_{2i} are the signal intensity and the spin-spin relaxation time of the i component. Osmotic pressures of FA dilute solutions were measured by Löser-OM806 osmometer (Löser Messtechnik, Germany). The UV-Vis absorption spectra were recorded by a UV-Vis spectrophotometer (Specord 250 Plus, Analytik Jena Corporation, Germany). DSC measurements were performed with a calorimeter (DSC-Q20, TA Instruments, United States). The RBCs were counted by the automated cell counter (Countstar, Shanghai RuiYu Biotech Co. Ltd, China). The absorbance at 415 nm for cell recovery analysis was measured by microplate reader (SpectraMax i3 spectrophotometer, Molecular Devices, United States). Flow cytometry analysis was performed on BD FACSAria SORP cytometer (BD Company, United States).

Ice recrystallization experiments

Firstly, various desired concentrations of FA PBS solutions were prepared. Ice recrystallization ability analysis was carried out via splat cooling method, as previous reports(Bai et al., 2017; Knight et al., 1988). Briefly, a droplet of about 10 μL of FA PBS dispersion was dropped onto the surface of coverslip sat on the Linkam cryostage with the setting temperature of – 60°C from about 1.2 m height above it. The droplet froze instantly and formed a thin ice flake. Then the temperature of the cryostage was increased to – 8 or – 6°C at a rate of 5°C min^{-1}. Subsequently, the ice flake was annealed at – 8 or – 6°C for 45 min. Afterwards, the polycrystalline ice was photographed with a digital camera fitted to the microscope. The images were processed using ImageJ, obtaining the grain sizes of ice crystals. In brief, ten largest ice crystals were chosen and the largest lengths in any axis of the ice crystals were recorded. The above process was repeated for three times and the mean value was calculated, giving the MLGS.

Single ice crystal growth experiments

The growth process and morphology of single ice crystal in FA solution of different concentrations were observed by an Otago Nanoliter Osmometer, which method was referred to in previous reports(Braslavsky and Drori, 2013). The growth and shape of single ice crystal in pure water were also observed as a contrast. Briefly, the device was firstly calibrated using ultrapure water and NaCl solution, respectively. Then, submicroliter volume of FA solution or H2O was injected into a temperature-controlled sample holder full of immersion oil Type B using a microsyringe connected with a capillary tube. Afterwards, the temperature-controlled sample holder was cooled quickly to make the droplet immersed in the oil freeze. Subsequently, the droplet was warmed slowly until a single ice crystal remained and the ice crystal size was kept about 15 μm in diameter. Then the small ice crystal was kept at a certain temperature for about 20 s with no growing and no melting. That temperature at which the small ice crystal didn't grow or melt is determined to be the melting temperature (T_m). Then the temperature was decreased to a desired value (T_t) and kept. The growth of the single ice crystal during this process was recorded by a high-speed camera.

Supercooling temperature (ΔT) is calculated by subtracting T_f from T_m. Each growth procedure was repeated at least three times.

Ice affinity experiments

The ice affinity experiment is inspired by the AFP purification method (Kuiper et al., 2003). Briefly, the apparatus consists of a temperature-controllable cooling circulation system and a hollow cold finger, jacketed cup connected with the circulation system, as shown in Figure S2. The flask containing FA solution (1 mg mL^{-1}, 80 mL) was immersed in the jacketed cup of low temperature bath with magnetic stirring, and the cold finger with seeded ice was lowered into the pre-chilled FA solution. By adjusting the temperature of the cooling circulation system, the ice growth rate can be regulated. About 2 mL ice was formed for every set temperature. Then, the ice was melted and measured for the FA concentration by UV-Vis spectrophotometer.

Ice formation observation during rapid cooling stage

10 μL liquid sample was dropped on the center of a clean coverslip and then was covered by another clean coverslip to make the liquid spread between the two coverslips. Afterwards, the two laminated coverslips with liquid between them were put on a cryostage and cooled from room temperature to − 120°C at varied cooling rates (typically ≥ 20°C min^{-1} to simulate the rapid cooling condition during cryopreservation in this work). Then the frozen sample was photographed with a digital camera fitted to the microscope. The images were then processed using Image J, obtaining the grain sizes of ice crystals.

Fractionation of FA

As the structural complexity of the crude FA, we made a fractionation according to the molecular weight. Briefly, the crude FA was dissolved into water and firstly fractionated using a stirred cell (Millipore Amicon) with an Ultracel membrane (molecular weight cutoff: 1 kDa) inside it under a pressure of about 0.4 MPa, obtaining two fractions with the molecular weight of > 1 KDa (the remnant in the cell, denoted as FA>1KDa) and < 1KDa (the filtrate), respectively. Then the filtrate was further fractionated through flash column chromatography on silica gel using a gradient of ethanol (Fraction 1, very tiny amount), methanol/ethanol with volume ratio of 4:1 (Fraction 2) and water (Fraction 3) as the eluent. The main component of Fraction 2 and 3 were denoted as the format of $FA_{\overline{M}_n}$, where $\overline{M}_n$ is the number-average molecular weight and is measured based on the colligative property of osmotic pressure.

RBC-related experiments

Preparation of RBCs

Before the RBCs cytocompatibility and cryopreservation experiments, the purchased sheep RBCs were centrifuged at 275 g for 5 min at 4°C. Then the supernatant was replaced with equal volume of PBS solution. This process was repeated three times to ensure that any residual plasma or saccharides were removed thoroughly. The prepared sheep RBC dispersion was used timely and was stored in 4°C refrigerator for a maximum of 5 days when not used.

Cytocompatibility assay

Cytocompatibility assay of RBCs was carried out by referring to the reported papers(Bai et al., 2017; Mitchell et al., 2015). To ensure the sufficiently blending, double the desired concentrations of FA PBS solutions were firstly prepared and adjusted to neutral (pH = 7.4) by NaOH, and then mixed with equal volume of RBC PBS dispersion. Afterwards the samples were vortexed gently and preserved at 4°C refrigerator for 24 h before the cell recovery measurement of RBCs.

Cryopreservation of RBCs with FA

The cryopreservation experiments of RBCs were performed by referring to the previous reports(Deller et al., 2014). Firstly, the sample preparation procedure was the same with that of cytocompatibility assay. Then all the samples with the final packed cell volume of 10% and final desired FA concentrations were then plunged into liquid nitrogen for 2.5 h. Subsequently, the samples were put in 4°C refrigerator for 150 min or 45°C water bath for 1 min to thaw. Afterwards, the samples were measured for the post-thaw cell recovery immediately or stored in 4°C refrigerator for different time before the measurement of the cell recovery/viability. For comparison, commercial cryoprotectant HES were also dissolved in PBS solution and used as cryoprotectant performed as above. Note that to avoid the possible influences of the difference among

RBC samples, each test condition was repeated three times in different batches, and in every batch all the test and control groups are included.

Cell recovery measurement

40 μL sample after cytocompatibility or cryopreservation experiments was added to 400 μL PBS solution and centrifuged at 275 g for 5 min at 4°C to remove the intact cells. Afterwards, the absorbance (at 415 nm, the maximum absorption peak of hemoglobin) of the supernatant was measured by microplate reader, assessing the haemolysis extent, thus the cell recovery. Note that the real absorbance value of haemolysis was obtained by subtracting the absorbance of FA at the same condition from the measured absorbance value above, to eliminate the absorbance interference of FA at 415 nm. The absorbance of FA at the same condition was obtained as following. Exactly the same control experiments as cytocompatibility/cryopreservation assays but replacing the prepared RBCs with PBS solution were carried out. Then the FA PBS solutions were centrifuged and measured for UV-Vis absorbance exactly the same way as RBC supernatants. 100% haemolysis samples were prepared by osmotic shock, *i.e.*, adding 500 μL H_2O to a 500 μL prepared RBC dispersion and then shaking it violently. 0% haemolysis samples were prepared by adding 500 μL PBS to 500 μL prepared RBC dispersion and leaving untreated exactly the same environment as the cytocompatibility/cryopreservation experiments. Note that for every batch experiment, 100% and 0% hemolysis samples were prepared freshly. Cell recovery (%) was calculated by subtracting the attained haemolysis (%) from 100 (%). To evaluate the cell recovery of the thawed RBCs more strictly, we further measured the cell recovery at various post-thaw culturing time through counting the intact RBCs by a hematology analyzer (Bowlinman, BM830, Beijing Bowlinman Sunshine Science & Technology Co., Ltd). Cell recovery measured by this method was calculated as the ratio of intact counts of the thawed RBCs to the counts of RBCs initially frozen (cell recovery% = $\frac{cell_{intact}}{cell_{frozen}} \times 100$).

Cell viability measurement

The viabilities of the thawed RBCs were further studied by flow cytometric assay using a lipophilic fluorescein derivative—calcein-AM, which can passively penetrate the cell membrane of viable cells and then be converted to the polar and membrane-impermeable calcein by intracellular esterases. The generated calcein can emit bright green fluorescence (E_x = 490 nm, E_m = 515 nm) and be retained by cells with intact membranes. For the dying or damaged cells of compromised membrane integrity, the unhydrolyzed calcein-AM or the fluorescent calcein can be rapidly expelled from cells. The experimental procedures are performed by referring to the reference(Bratosin et al., 2005). Briefly, the purchased calcein-AM was diluted using PBS buffer into the concentration of 100 μM as the working solution. Then the cleaned RBCs after thawing (8×10^5 in 400 μL PBS buffer) were incubated for 45 mins with 20 μL calcein-AM working solution at 37°C in dark. Afterwards, the sample was analysed immediately for the calcein fluorescence retention in cells by flow cytometer with the channel of FITC. The blank control RBCs (have not been frozen) with and without the above staining procedure were also performed the flow cytometric analysis as the control. Each sample was tested at least three times. Note that before the measurement, we examined the reliability of this method by analyzing the fluorescence retention of RBCs with various viabilities, which were realized by incubating the fresh RBCs with noxious sodium azide (0.05%, in PBS buffer) for different time (Figure S13). The cell viability of the thawed RBCs is quantified by defining the viability of the blank control RBCs which have not been frozen (*i.e.*, RBCs stored at 4°C for the same time as the experiment group) as 100%. Specifically, based on the flow cytometric analysis (see Figure S13 for the typical data), the mean fluorescence intensity (*MFI*) was used to quantify, which is usually adopted for cell viability analysis: cell viability (%) = $\frac{MFI_{thawed\ cells}}{MFI_{blank\ control}} \times 100$.

Uptake situation of FA by RBCs

The uptake situation of FA by RBCs was investigated through monitoring the variation of FA concentration compared with the control group. Specifically, the experimental group was prepared by mixing RBC dispersion (packed cell volume of 10%) with equivalent volume of FA PBS solution (40 mg mL^{-1}). The control group was the identical RBC (packed cell volume of 5%) and FA (20 mg mL^{-1}) samples without mixing. After incubation at room temperature for 15 min, both the experimental and control groups were centrifuged at 275 g for 5 min at 4°C. Then the absorbances of the supernatants were measured. For the experimental group, the absorbance was labeled as A_{RBC+FA}; for the control group, the absorbance was labeled as $A_{RBC} + A_{FA}$. The absorbance results were compared to assess whether FA was taken by RBCs. The uptake ratio was calculated as: uptake (%) = $\frac{A_{RBC} + A_{FA} - A_{RBC+FA}}{A_{FA}} \times 100$. To further explore whether FA attaches on membranes or permeate into RBCs, the obtained precipitates were mixed with pure water to make the

RBCs lysed, and then the mixtures were centrifuged at 15644 g for 20 min at 4°C to separate the cell membranes (precipitate) and intracellular fluid (supernatant). The control group was treated in the same way. Finally, the absorbances of both the supernatant and precipitate were measured.

Molecular dynamics simulations

The all-atom simulations were performed on the Gromacs-5.1.4 software package(Abraham et al., 2015). The structures and force field topologies of two molecules (FA: ATB molid of 22656 and Suc: ATB molid of 715061) were generated by Automatic Topology Builder (https://atb.uq.edu.au) with GROMOS 54a7 parameters.(Malde et al., 2011; Stroet et al., 2018) The molecule was firstly aligned with a simulation box with size of $4\times4\times4$ nm^3 and centered in position. The system was subsequently solvated by 2150 waters with type of *SPC*, making the mass density of the system approximately as 1000 $kg\cdot m^{-3}$. An energy minimization in 5000 steps was conducted by the steepest descent method. In the equilibration process, a force constraint of 1000 $kJ\cdot mol\cdot nm^{-2}$ in three dimensions was defined on the α-carbon atoms to fix the positions of molecules. A cutoff-scheme function was used with the Coulomb interaction and Lennard-Jones interaction decrease to zero from 0 to 1.2 nm. The temperature path using Berendsen thermostat method (Berendsen et al., 1984) was conducted with a reference temperature of 320 K and a time constant of 0.5 ps. The pressure coupling was implemented using the Parrinello−Rahman method (Parrinello and Rahman, 1981) in a "isotropic" coupling type, with a reference pressure of 1.0 bar, compressibility of 4.5×10^{-5} bar^{-1} and a time constant of 2.0 ps. The periodic boundary condition was applied. The time step of the simulation was set as 1 fs, and the total simulation time duration was set to 50 ns. The simulation snapshots were captured by the VMD-1.9.2 software.

Statistical analysis

All calculations and fittings were determined using software OriginPro Learning Edition. One-way analysis of variance (ANOVA) was used for statistical significance analysis in software SPSS Statistics. Significance level of difference of the mean is 0.05.